

Experimental characterization and modeling of energy dissipation in reinforced concrete beams subjected to cyclic loading

R. Crambuer, B. Richard & N. Ile

CEA, DEN, DANS, DM2S, SEMT, Laboratoire d'Etude Mécanique Sismique, F-91191 Gif-sur-Yvette, France.

F. Ragueneau

LMT - ENS-Cachan, France



SUMMARY:

This paper presents a series of three points bend tests that was realised during the SMART 2008 campaign. The results presented here are largely derived from field measurements by image correlation. Particular attention was given to the evolution of cracking and to the effects of prior damage on the evolution of the damping ratio. For each cycle, an equivalent viscous damping and multiple damage indices were determined. Indeed, the analysis of the local behaviour of a crack (opening, closure, propagation, sliding) allows a correlation between the energy dissipation and the nonlinear behaviour of the material. A numerical campaign was perform using a nonlinear cyclic model that takes into account these phenomena This campaign should make it possible to highlight the influence of the different source of dissipation on damping.

Keywords: Damping, 3 point bending tests, image correlation, isotropic damage model, reinforced concrete

1. INTRODUCTION

The analyses of the SMART 2008 campaign (Juster-Lermitte 2010, Crambuer 2011) (EDF-CEA) revealed the difficulties to quantify and even more to model the damping phenomena that appears in reinforced concrete (RC) structures under seismic solicitations. Both experimental and numerical analyses of damping in structures submitted to seismic loading are needed in order to understand the mechanisms involved in the energy dissipation phenomena. It is also a necessity to be able to quantify these phenomena in order to model them. To do so it is necessary to build a suitable experimental database.

Many experimental campaigns have been carried out in the last decades in order to understand the causes of damping in RC structures. Most of those tests where realised on structural elements and consisted on hammer shock tests (Capozucca 2009). A four point bending test was performed on a beam in order to achieve different levels of damage (Salzmann 2002). Then, for each level, the beam was taken from the assembly, was suspended and hammer test were perform on several points. With such a test campaign Salzmann highlighted the influence of the reinforcement ratio on the dissipation phenomena. Other tests where performed on columns: a horizontal quasi static displacement load was applied on the top (Carneiro 2005) or at the middle of the specimen (Tassios 2006). In the tests of (Brown 2009), a cyclic displacement load was applied, with increasing displacement. Generally two or three cycles were performed at each level in order to stabilise the damage and to be able to calculate the damping at each level. (Petrini 2009) performed seismic tests rather than quasi static tests.

The campaign presented here consisted in performing three point bending tests on eight beams. These beams exhibited four different horizontal reinforcement ratios (from 0.5% up to 2%). In quasi static loading, the loads applied to the beam are generally controlled in displacement and consisted in cycles of increasing displacement. In this campaign one beam of each configuration was tested with a first cycle at about 80% of its maximum force, in order to test precracked beams. Such a loading case is interesting because it could represent the behaviour of a structural component after a main seismic

shock and its behaviour to further lower amplitude seismic excitation. The other beams loading are totally different. An important damage level is achieved and then smaller cycles are applied. To catch the crack pattern evolution during tests image correlation (Hild 2007) were performed on each beam. To catch the multiple source of dissipation sophisticated inelastic model were used for the numerical campaign, in particular for the concrete. This campaign highlights the phenomena that generate the dissipation, a numerical campaign, with complex model, have been realised in order to model correctly the dissipation using complex isotropic damage model.

To reach all these objectives the paper is outline as follows. In section 2, the experimental campaign is exposed and the experimental setup is emphasized. An attention is also paid to the equivalent damping ratio method. Then the experimental results are presented and discussed in order to highlight the mechanism that appears during the tests. In section 3, the numerical campaign is exposed. The isotropic damage model used to model the concrete is described with particular attentions to the mechanisms that are taken into account. Then the multifiber structural modelling is detailed and its use is justified. Finally the numerical results are compared to the experimental ones.

2. EXPERIMENTAL CAMPAIGN

2.1. Experimental setup

Eight rectangular RC beams were tested with different longitudinal reinforcement steel ratio presented in Table 1. They were cyclically tested for different loading histories under forced and then displacement controlled conditions. The beam specimens are 1.65 m length and have a 0.22 m x 0.15 m cross-section area (Crambuer 2012). The reinforcement details are presented in Fig.1. The material considered at the specimen design phase were a regular concrete class C30/37, with reinforced steel grade of B500B, the average concrete strength obtained on samples are summarised in Table 1.

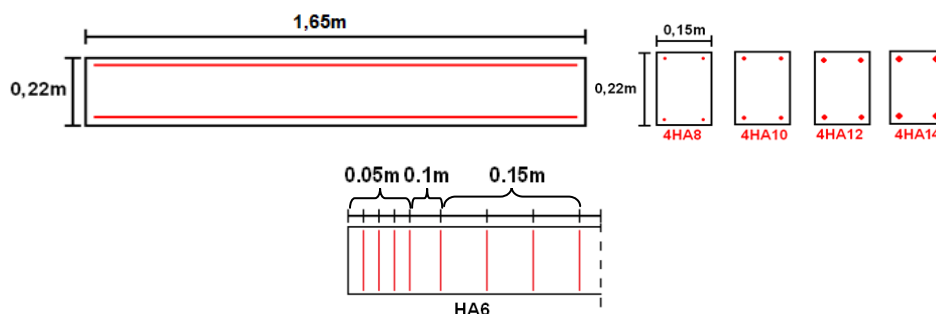


Figure 1. RC beam specimen dimensions and reinforcement detailing

Fig. 2 (a) shows the setup adopted for the experimental testing including the vertical MTS actuator used to apply the load with a capacity of 160kN and ± 170 mm stroke. The strength is transmitted to the beam by a jaw connected to the beam. The beams were designed to be tested with a simple three-point bend setup in both directions of loading. The hinge device used in this campaign, and presented Fig. 2 (b), was developed during (La Borderie 1991) campaign. They allow making the hypothesis of a hinge connection. This hypothesis is verified if the behaviour of the support system remains elastic. In this setup it means that the maximal hinge device rotation should be not greater than 0.2rad.

In order to calculate the equivalent viscous damping it appears that it was more interesting to control the force instead of the displacement. The problem was that you can't access the post-pic behaviour of the beam with a force controlled load. Until the maximum force obtained in a cycle was smaller than 80% of the expected maximum force of the beam, the load was controlled in force. For the following cycle the load was controlled in displacement.

Digital image correlation (DIC) was obtained using a Canon 60D camera. The studied zone of an image is named the Region Of Interest (ROI) Fig. 4 shows a typical dimension of a ROI and the corresponding resolution. The width of this zone is 560 mm. The image resolution is $3456/560 = 6.17$

pixels/mm. The system used to apply the alternate loading is shown also in Fig. 4. We considered here the ROI as the entire photographed zone to be analyzed by the DIC technique. This technique of correlation allows us to characterise in a very precise way displacements and deformations starting from a reference digital image (Hild 2007). One obtains the Displacement and strain field in the ROI. Therefore, it is possible to determine the cracks opening at each moment a picture is taken. With DIC one can know the evolution of the cracking states of the ROI area during the experiment. The image correlation is done by CorreliLMT software (Hild 2002).

For each series of beams two different loadings were applied as presented in Table 1 (Crambuer 2012). The uncracked loading consisted in applying progressive damage level corresponding to the first crack, limited damage, average damage, and one or several important damage. For each damage level the loading consisted in five cycles of loading as described in Fig. 3(a). The pre-cracked loading consisted in applying directly an important damage to the beam. Then progressive damages were applied to the beam from very low level to very high level as described in Fig. 3(b).

Table 2.1. Specimen specifications and loading characteristics

Series	Beam	f_{cm} (MPa)/error(%)	f_{tm} (MPa)/error(%)	Steel ratio (%)	Loading case
1	HA8-L1	32/0.6	2.6/0.1	0.67	Uncracked
	HA8-L2				Pre-cracked
2	HA10-L1	34/2.5	2.7/10	1.05	Uncracked
	HA10-L2				Pre-cracked
3	HA12-L1	38/12.3	2.7/1.6	1.51	Uncracked
	HA12-L2				Pre-cracked
4	HA14-L1	32/5.2	2.7/16	2.05	Uncracked
	HA14-L2				Pre-cracked

f_{cm} – mean concrete compressive strength
 f_{tm} – mean concrete tensile strength

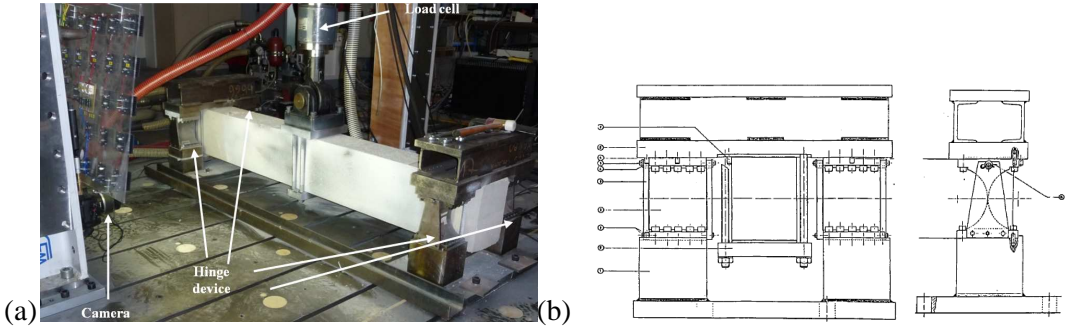


Figure 2. Testing setup: (a) General view (b) hinge device scheme (Laborderie 1991)

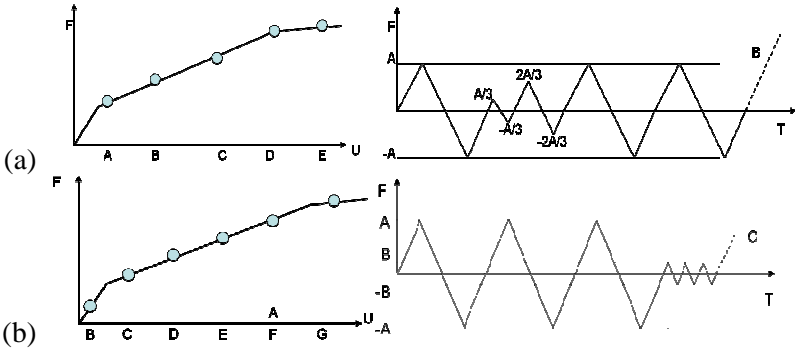


Figure 3. Description of loadings: (a) Uncracked and (b) Pre-cracked

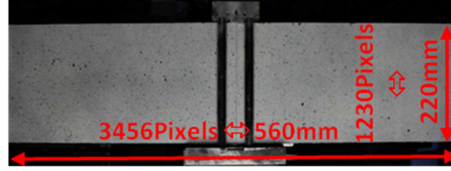


Figure 4. An example of a Region of Interest (ROI) and the corresponding resolution

2.2. Equivalent viscous damping ratio

For the case of perfectly symmetric hysteretic response and corresponding closed loop, the equivalent viscous damping ξ_{eq} can be given by the Eqn 2.1, where A_h stands for the dissipated energy within a given cycle, A_e is the area of the deformation energy stored in the equivalent linear elastic system having an effective stiffness equal to $k_{eff} = V_m/\Delta_m$.

$$\xi_{eq} = \frac{A_h}{4\pi A_e} = \frac{A_h}{2\pi V_m \Delta_m} \quad (2.1)$$

In this campaign the loading and the concrete properties lead to asymmetric hysteretic response. It is mainly due to the cracks opening. One also has to take into account that the loops are not all closed due to the evolution of the structure during the cycle. For all these reasons the Equation 6 couldn't be used in this study.

- However, using the work of (Jacobsen 1960) and according to (Varum 2003), the equivalent viscous damping can be evaluated for each half cycle of the force-displacement curves as described next: First, each half-cycle is determined by two successive zero force point.
- For each half cycle the maximum generalised displacement D_m and generalised force V_m are determined in order to calculate the area of the deformation energy
- For each half-cycle, one performs the integral of the force-displacement curve which is equivalent to the dissipated energy (A_h) and leads to the A_{half_loop} value.
- Finally, the equivalent damping ratio is calculated in each half-cycle as described in Eqn 3.2

$$\xi_{eq} = \frac{1}{\pi} \frac{A_{half_loop}}{V_m \Delta_m} \quad (3.2)$$

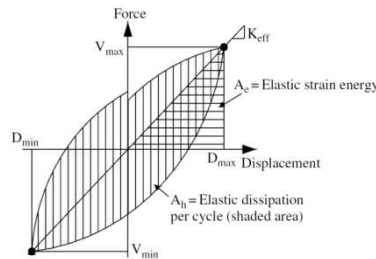


Figure 5. Damping for an hysteretic half cycle (Petrinia 2008)

2.3. Experimental results

The different reinforcement steel ratios are expected to reveal different failure mechanisms and to have a great influence on the beam maximum capacity. A problem appears during the test of the beam HA14-L1. One of the hinge devices was partially blocked when we applying the loading, so the behaviour of this beam will not be presented here.

2.3.1. Global behaviour of the eight beams

The overall capacity of the beams is presented in Fig.6. It appears clearly that the capacity of the beams depends on the steel ratio as it is widely accepted. It is interesting to notice that the loading

history has a minor effect on the ultimate capacity. This confirms the interest of monotonic loadings to determine the material parameters for the predictive models to be used in numerical analyses. For every beam one can see that:

- For lower displacements, in the first part of the curve, the force increases proportionally to the displacement and the stiffness gradually reduces due to the appearance of cracks in concrete
- For the most important displacements the force remains constant and the dissipation comes essentially from the steel.

The difference between the beams of the first series is due to the collapse of beam HA8-L2 during the test. Table 2.2 presents the force-displacement response for the beams of the series 2. One can note the influence of the loading history on the beam behaviour.

- For the uncracked beam the stiffness decrease for each series of cycle.
- For the precracked beam the stiffness decrease a lot during the first cycle then it remains constant until the load reach higher value. Then the stiffness decrease progressively like in the other beam

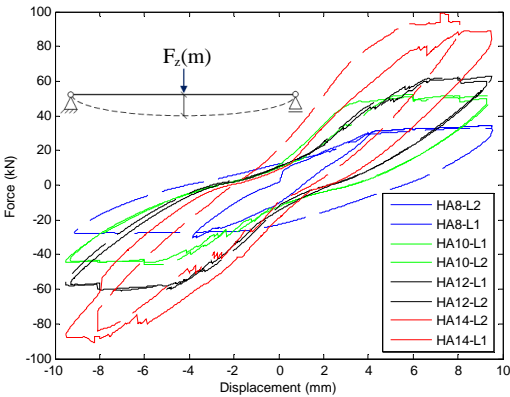


Figure 6. Force-displacement behaviour of the 8 tested beams

Table 2.2. Force displacement curve of the series 2 beams.

	Uncracked	Precracked
Series 2		

2.3.2. Cracks analyses

Table 2.3 presents the cracking patterns at the end of each test.

- The series 1 and 2 beams exhibit vertical cracks. This kind of crack is due to bending solicitation. There is only a few crack it means that there is not enough horizontal reinforcement. The beams behave like concrete beams.
- The series 4 beams exhibit of diagonal cracks. This kind of crack is due to bending and shear solicitation. There is a lot of crack which means that the reinforcement takes the stress back when cracks appear.

- The series 3 beams exhibit vertical and diagonal cracks. Their behaviour is a mix of the other series behaviour. It is a classic behaviour of RC elements with an appropriate reinforcement ratio.

It is also to be noted that all the cracks appear close to the stirrups position. Table 2.4 presents the evolution of the cracking patterns in the ROI during the test for the beam HA10-L2. The two images on the top represents the first cycle that pre-cracked the structure. One can see in the cycle at $\pm 35\text{kN}$ and the second one at ± 50 that the cracks that re-open for these cycles were all created at the first $\pm 50\text{kN}$ cycle. All the cracks opens more largely for the $\pm 8\text{mm}$ cycle.

Table 3.2. Cracking patterns at the ends of the test

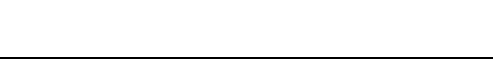
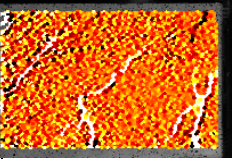
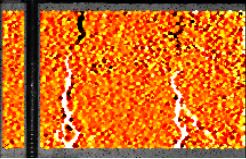
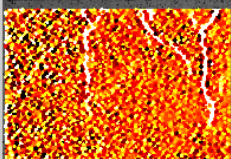
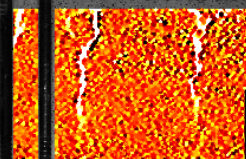
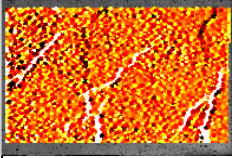
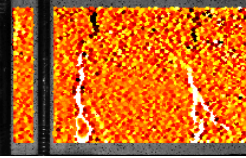
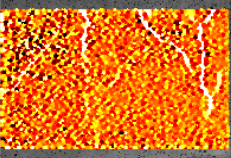
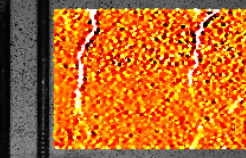
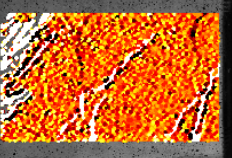
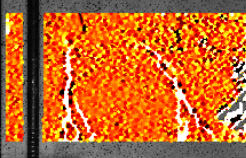
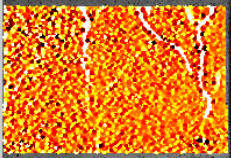
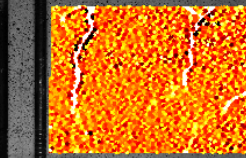
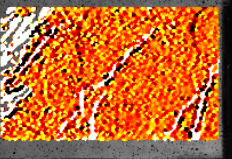
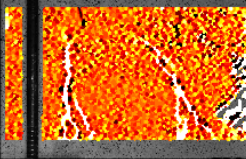
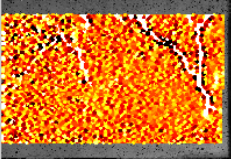
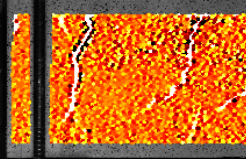
	Uncracked	Precracked
Serie 1		
Serie 2		
Serie 3		
Serie 4		

Table 3.3. Evolution of cracking in the ROI of beam HA10-L2

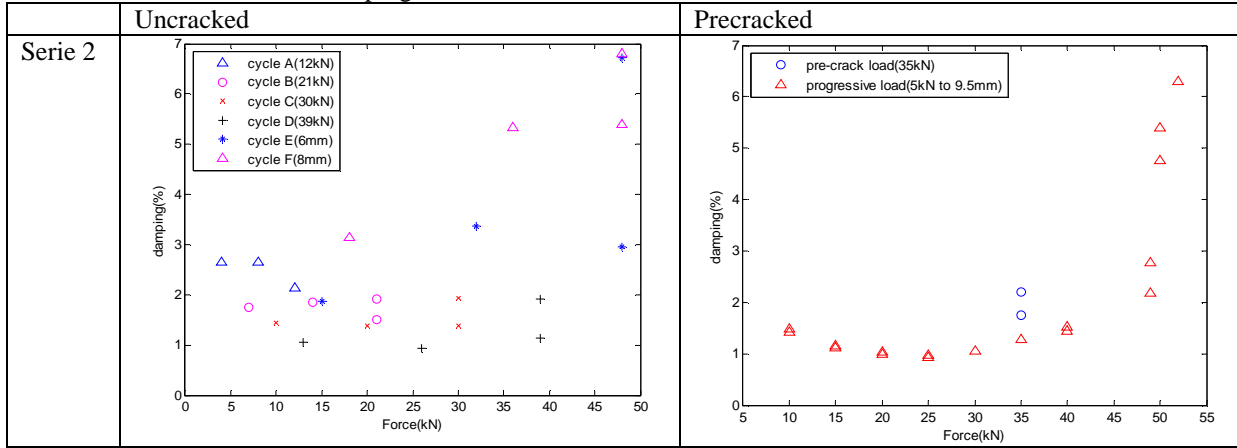
	Positive displacement		Negative displacement		
$\pm 50\text{kN}$					-0.0100 -0.0089 -0.0079
$\pm 35\text{kN}$					0.0068 0.0058 0.0047 0.0037 0.0026 0.0016
$\pm 50\text{kN}$					-0.0005 0.0005 0.0016 0.0026 0.0037 0.0047
$\pm 8\text{mm}$					0.0058 0.0068 0.0079 0.0089 0.0100

2.3.3. Damping evolution

Table 3.4 exhibits the damping evolution of the beams of series 2. The influence of the loading history on damping appears clearly. The precracked beams present lower values of damping for every cycle under the precracked value. With this loading important cracks are create during the first cycle and then they just partially reopen and reclose. In the other beam new or extended crack appear at each new damage level. This new cracks dissipated more.

Two main behaviours appear clearly, up to 35kN. Damping is quite low, less than 4%. Most of the dissipation comes from the concrete; a small part comes from the connections. After 35kN, damping increases due to the steel hardening. In this part the damping values are very close for the two beams.

Table 3.4. Evolution of the damping of the series 2 beams



3. NUMERICAL ANALYSIS

3.1. Isotropic damage model for concrete under cyclic loading

This constitutive model is expressed within the framework of isotropic continuum damage mechanics and plasticity for seismic applications. It is based on the following observations (Mazars 1990). In tension, quasi-brittle materials exhibit localized cracking although in compression diffuse (or smeared) cracking appears. Therefore, isotropic damage is used in tension and plasticity is used in compression. The use of plasticity in compression is frequent in the field of soil mechanics when nonlinearities and permanent strains must be described. Tension and compression can be split into two distinct parts by considering the sign of the Cauchy stress. Since hysteretic phenomena are related to localized cracking, this mechanism is considered in tension, allowing a realistic description not only of hysteretic loops but also of permanent strains in tension. The unilateral effect is also taken into account using a closure function which ensures the continuity stress/strain relation whatever the loading path. With these assumptions, one can state that the behaviour of a representative elementary volume is accurately represented in tension (brittleness, hysteretic loops and permanent strains) and globally described in compression (nonlinearity and permanent strains).

The proposed isotropic damage model is built within the thermodynamic framework. The best known lies in expressing this potential as the Helmholtz free energy that a strain-based formulation or as the Gibbs free enthalpy, that is a stress-based formulation (Lemaitre 1985). Recently, a new class of constitutive models based on a state coupling between damage and friction has been developed to describe the behaviour of quasi-brittle materials subjected to cyclic loadings (Ragueneau 2000, Richard 2010). The potential can be expressed according to Eqn. 4.1:

$$\rho\psi = \frac{1}{2}\{(1-d)(\varepsilon - \eta\varepsilon^\pi - \varepsilon^p)E(\varepsilon - \eta\varepsilon^\pi - \varepsilon^p) + d(\varepsilon - \eta\varepsilon^\pi - \varepsilon^p)E(\varepsilon - \eta\varepsilon^\pi - \varepsilon^p) + \gamma\alpha^2\} + H(z) + R(p) \quad (4.1)$$

Where the ρ is the material density, ψ the Helmholtz free energy, E the Young modulus and ε is the axial strain, d is the scalar damage variable, ε^p is the permanent strain, η is the closure variable, ε^π is the internal sliding strain, γ is the kinematic hardening modulus, α is the kinematic hardening variable, z is the isotropic hardening variable, p is the cumulative plastic strain and H and R are two consolidation functions.

The constitutive laws show interesting properties such as the representation of hysteretic loops and permanent strains. The unilateral effect is taken into account through a closure function, ensuring not only the continuity of the stress/strain relation but also a full stiffness recovery when switching from

tension to compression. The Cauchy stress could be described in Eqn. 4.1:

$$\sigma = (1 - d)E(\varepsilon - \varepsilon^p) + dE(\varepsilon - \varepsilon^p) = E(\varepsilon - \varepsilon^p) \quad (4.2)$$

The numerical implementation of the above isotropic damage model in uniaxial stresses case is applicable for multifibre modelling. A complex loading path is considered to emphasize the numerical robustness of the proposed constitutive model as well as the relevancy of the local concrete behaviour description. The material parameters used to simulate this loading path are presented in table 3.1 they were selected according to the experimental data. The loading is displacement controlled to capture the post-peak regions. In tension, the model exhibits a brittle behaviour as well as hysteretic loops. Moreover, when switching from tension to compression, the cracks are progressively closed up to recover the initial stiffness. In compression, permanent strains are taken into account as the only dissipative mechanism is plasticity. A linear behaviour is recovered when unloading. The cracks are also re-opened progressively when a tension stress state appears after carrying out a compression (Fig. 8). The hysteretic stress–strain relationship of reinforcing steel is described by the nonlinear model of Menegotto and Pinto (Menegotto 1973), as modified by (Filippou 1983) to include the isotropic strain hardening effects (Fig. 8), the model accounts for the Bauschinger effect under cyclic loads.

Table 3.1. Material parameters

Symbol	Parameter	Identified value
E	Young's modulus	28000 10^6 Pa
ν	Poisson's ratio	0.2
Y_0	Initial threshold for damage activation	82.82 $J.m^{-3}$
A_d	Brittleness coefficient	9.0 $10^{-3} J^{-1}.m^3$
γ	Kinematic hardening modulus 1	3.0 10^9 Pa
a	Kinematic hardening modulus 2	8.0 $10^{-6} Pa^{-1}$
σ_f	Mean closure stress	-3.0 10^6 Pa
σ_c	Compressive strength	-10.0 10^6 Pa
a_R	Plastic hardening modulus 1	4.0 10^{10} Pa
b_R	Plastic hardening modulus 2	600

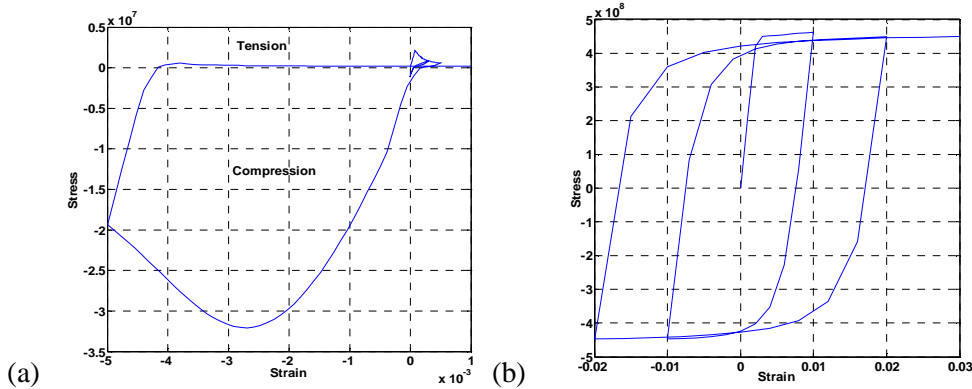


Figure 8. Stress-strain Response for concrete (a) and steel (b) with the experimental parameters

3.2. Multifibre structural modelling

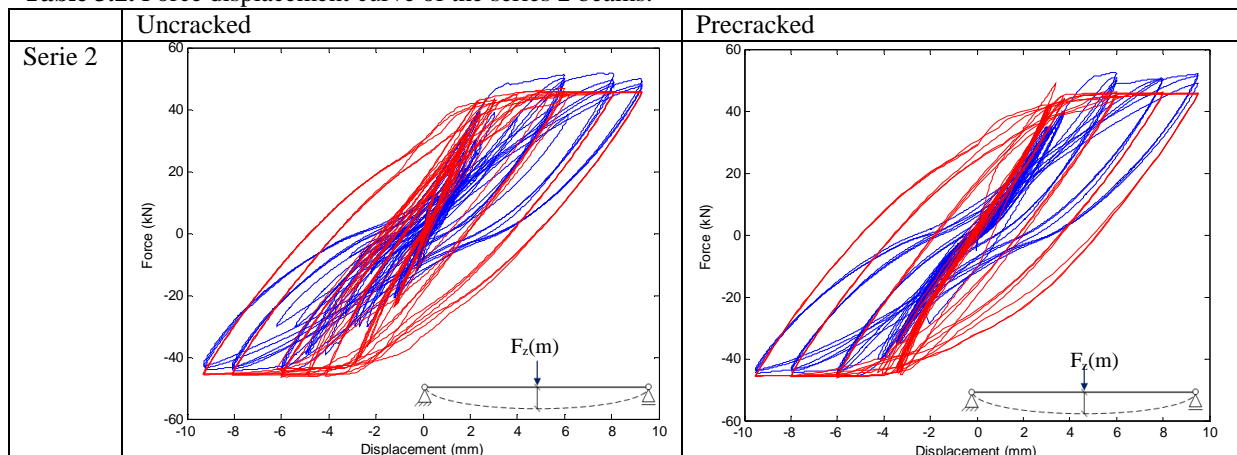
As will be seen in the following, finite element numerical simulations were capable to describe quite well the complex behaviour of this structural element. In this study the displacement of the beam only occurs in a plan and there is no out of plane displacement. Its behavior is a classic beam behavior. Since, the computational costs of complete 3D approaches are really important, it was decided to use an intermediate structural discretisation (between complete 3D approach and macro-element method). A really good method for such elements and loads is to use a multifibre approach. It introduces a low number of degree of freedom insuring global convergence in a fast way. The classical Timoschenko beam model is perfectly suited for this kind of application. It keeps the refined constitutive equation at

the local level but, due to the beam kinematics, those are implemented only in their uniaxial features. The kinematics hypothesis assumes no distortion or warping of a cross-section. In a multifibre nonlinear model the flexural and axial behavior are coupled. To optimize the simulation cost, only one half of the beam was model, due to the symmetric behavior. The absence of out of plan displacement leads us to a mesh with only one element in depth.

3.3. Numerical results

During the experimental tests, energy dissipation in beams, is due to cracking of concrete and yielding of the reinforcement steel bar. These two phenomena have to be modelled correctly in order to fit the experimental results. In this study it seems that the concrete behaviour is correctly taken into account (table 3.2) but for the most important cycles, corresponding to the steel yielding the pinching effect doesn't appear in the model. This could be a consequence of the fact that the numerical model assumes perfect bond between steel and concrete. It seems that this phenomenon appears mainly during unloading when cracks are open on both sides, before they close at one face. The pinching effect could also have been underestimated (overprediction of loop "fatness") due to the lack of shear deformation modelling in the fibre approach.

Table 3.2. Force displacement curve of the series 2 beams.



4. CONCLUSIONS

A study of an experimental and numerical campaign on RC beams has been presented. Eight beams have been tested in a cyclic three point bending setup. They all have the same dimensions but different longitudinal reinforcement ratio. Two different kinds of loads have been applied in order to study the influence of the loading history. The measurement setup used a digital image correlation technique that gives full field information in terms of displacement and strain. For each cycle the equivalent viscous damping has been calculated.

The numerical campaign uses an isotropic damage model that takes into account damage and isotropic hardening, internal sliding and kinematic hardening, plasticity and the unilateral effect. To limit the computational time, in order to be able in the future to perform seismic probabilistic simulation, multifibre structural modelling was used. Comparisons between experimental and numerical results were generally satisfactory; for higher damage level however, the numerical model needs some improvements in order to be able to better predict the pinching effect which was observed experimentally.

AKNOWLEDGEMENT

The authors would like to thank the experimental team of LMT Cachan and in particular X. Pinneli for his help during the experimental campaign. This paper is based on research supported by the CEA, the LMT ENS

Cachan. Partial support was also provided by the EDF.

REFERENCES

- Baghiee, N. Esfahani, M., Moslem, K. (2009). Studies on damage and FRP strengthening of reinforced concrete beams by vibration monitoring, *Engineering Structures*, **31:4**, 875-893.
- Carneiro, J.O., deMelo, F.J.Q., Jalali, S., Teixeira, V., Tomas, M. (2006). The use of pseudo-dynamic method in the evaluation of damping characteristics in reinforced concrete beams having variable bending stiffness. *Mechanics Research Communication* **33:5**, 601-613.
- CAST3M – <http://www.cast3m-cea.fr>
- Crambuer, R., Juster-Lermitte, S., Ragueneau, F. (2011). Caractérisation expérimentale de la dissipation d'énergie de poutres en béton armé soumises à un chargement cyclique. *8^{ème} colloque national de l'Association Française de Génie Parasismique*. Art. **146**
- Crambuer, R. (2012). Mesures de dissipation hystérétiques par flexion 3 points sur poutres en béton armé. Internal report. France: LMT-Cachan (ENS Cachan/CNRS/Université Paris 6/UniverSud Paris).
- Elmenschawia, A., Brown, T. (2010). Hysteretic energy and damping capacity of flexural elements constructed with different concrete strengths. *Engineering Structure* **32:1**, 297-305.
- Filippou, FC, Popov, EP, Bertero, VV. (1983) Effects of bond deterioration on hysteretic behavior of reinforced concrete joints. *Internal Report No. UCB/EERC-83/19*, Earthquake engineering research center. Berkeley: University of California.
- Priestley, M. J. N. (1997). Displacement-based seismic assessment of reinforced concrete building. *Journal of earthquake engineering*. **1:1**, 197:192
- Hamam, R, Hild, F, Roux, S (2007). Stress intensity factor gauging by digital image correlation: Application in cyclic fatigue. *Strain* **43:3**, 181-192.
- Hild, F. (2002) CORRELI_{LMT}: A software for displacement field measurements by digital image correlation. Internal report. France: LMT-Cachan (ENS Cachan/CNRS/Université Paris 6/UniverSud Paris).
- Jacobsen, L. S. (1960). Damping in composite structures. *Second World Conference on Earthquake Engineering. Proceedings volume 2*, Tokyo and Kyoto, Japan, pp. 1029–1044.
- Juster-Lermitte, S., Crambuer, R, Ragueneau, F. (2010). Numerical and experimental analysis of a RC shear wall subjected to strong 3D seismic motions. *14th European Conference of Earthquake Engineering*. Art. **367**
- La Borderie C.(1991) Phénomènes unilatéraux dans un matériau endommageable : modélisation et application à l'analyse de structure en béton. *P.H.D. thesis*. Université de Paris 6.
- Mazars, J., Berthaud, Y., Ramtani, S. (1990). The unilateral behaviour of damage concrete. *Engineering Fracture Mechanics*, **28:7**, 857-874.
- Menegotto, M, Pinto, PE. (1973). Method of analysis for cyclically loaded reinforced concrete plane frames including changes in geometry and nonelastic behavior of elements under combined normal force and bending. *IABSE symposium on resistance and ultimate deformability of structures acted on by well-defined repeated loads, final report*.
- Mersseman, B. de, Millard, A. (1995) –Introduction du modèle Ottosen dans Castem2000, Formulation, Implémentation, *Internal Report CEA DMT/94-705*.
- Petrinia, A. L, Maggi C., Priestley, M. J. N., Calvi, G. M., (2008) Experimental Verification of Viscous Damping Modeling for Inelastic Time History Analyzes. *Journal of Earthquakes Engineering*, **12:1**, 125-145.
- Ragueneau, F., La Borderie, C., Mazars, J. (2000). Damage model for concrete-like materials coupling cracking and friction, contribution towards structural damping: first uniaxial applications. *Mechanics of Cohesive-Frictional Materials*, **5:8**, 607-625.
- Richard, B., Ragueneau, F., Cremona, C., Adelaide, L. (2010). Isotropic continuum damage mechanics for concrete under cyclic loading: Stiffness recovery, inelastic strains and frictional sliding. *Engineering Fracture Mechanics*, **77:8**, 1203-1223.
- Richard, B. (2011) Constitutive model for concrete under cyclic loadings: theory and numerical implementation in CAST3M v10 OSX. *Internal Report DEN/DANS/DM2S/SEMT/EMSI/RT/11-020/A*.
- Salzmann, A. (2002) Damping characteristics of reinforced and prestressed normal-and high-strength concrete beams, *P.H.D. Thesis*, Griffit University Gold Coast Campus
- Vintzileou, E., Tassios, T.P., Chronopoulos, M. (2007). Experimental validation of seismic code provisions for RC columns. *Engineering Structure*, **29:6**, 1153-1164.
- Varum, H. (2003) Seismic assessment, strengthening and repair of existing buildings, *P.H.D. thesis*. Aveiro : Civil engineering department, University of Aveiro.